Kovove Mater. 60 2022 151–161
DOI: 10.31577/km.2022.3.151

Development of a sustainable novel aluminum alloy from scrap car wheels through a stir-squeeze casting process

Al Maawali Jaber[1]*, Pradeep Kumar Krishnan[2]

[1] *Middle East College, Mechanical Engineering Department, Sultanate of Oman*
[2] *National University of Science and Technology, Mechanical & Industrial Engineering, Sultanate of Oman*

Received 23 December 2021, received in revised form 13 April 2022, accepted 17 May 2022

Abstract

Aluminum alloys are extensively finding applications in many industries, including automotive and aerospace, because of their lightweight. This research produced a novel aluminum alloy using a stir squeeze casting technique. Sustainability analysis of three competing processes to produce the alloy was carried out using Analytical Hierarchy Process (AHP) method. Scrap aluminum alloy wheels from cars were used as the matrix material. High entropy alloy (HEA) was used as the alloying element, with a total weight percentage of 2.6 %. Hardness, tensile and compressive strength tests were conducted for the developed alloy. An optical microscope, SEM, and XRD were used to analyze the microstructure. The produced alloy was heat-treated, and then mechanical properties and microstructure were compared before and after heat treatment. The results showed a significant improvement in hardness and compressive strength after heat treatment. This improvement is mainly attributed to the Si particle precipitation that occurred during the aging process.

K e y w o r d s: aluminum alloys, sustainability, squeeze casting, High Entropy Alloy (HEA), Analytical Hierarchy Process (AHP) method, T6 heat treatment

1. Introduction

Composites and alloys are developed because they are usually more robust and lighter than pure materials. For example, many of the components in the automobile industry are made from composites and alloys to reduce their weight [1]. Alloys are a mixture of two or more elements, also called a metallic solid solution. Mixing more than one element to form a solid solution changes the properties of the material, making it different from the original components. There are many examples of alloys, such as steel, brass, bronze, and different aluminum alloys. Each type of alloy has its unique properties, and each one of them is used for different applications depending on the required characteristics. The alloying process usually requires melting the component elements and mixing them to produce the new material.

There are different casting methods used to produce alloys. Squeeze stir casting is one of the casting methods used to develop aluminum alloys. Each casting method has its advantages and disadvantages, and different properties might be obtained from each method. For example, pores are more obvious in the gravity casting method because of present gases and insufficient feeding during casting [2]. In another study, a comparison between sand casting and gravity casting was conducted. It was shown that in sand casting, porosity and impurities were higher [3]. Another study compared sand casting and die (gravity) casting for scrap aluminum. The results showed that tensile strength and hardness were higher for gravity casting [4]. A study was conducted to compare squeeze casting and gravity casting. The results showed that gravity casting has more porosities than squeeze casting, affecting the mechanical properties. The hardness and the tensile strength of the squeeze casting were significantly higher [5]. An efficient method of improving the mechanical properties is to have pressure applied to the cast directly after it is poured into the die. The quality of the alloy highly depends on the squeeze pressure because it is necessary to decrease the percentage

*Corresponding author: e-mail address: jalmaawali@mec.edu.om

of porosity by reducing the formation of gas bubbles [6].

A sustainability analysis was done to compare three different casting processes to produce aluminum alloys. Suitability focuses on meeting the requirement of current and future generations, considering three main aspects: environment, economy, and social aspects. A concept scoring method was used to compare the squeeze casting method with sand casting and gravity casting. The three casting methods were compared in terms of mechanical properties, porosity, health and safety, energy consumption, and lead time. Each of these parameters is assigned to one of the three sustainability pillars: economy, environment, and social factors. In order to assign weights to these parameters, a survey was completed by three experts, and then the AHP method was used to analyze the survey results. The scores were given for these parameters for each casting method based on a review of the literature and expert judgments.

Using scrap aluminum as the main element instead of pure aluminum is advantageous for more sustainable production. The production of primary aluminum is a costly process, including the mining process of bauxite as well as the purification processes. Using scrap aluminum, however, will help in saving energy. It is cited that re-melting scrap aluminum will save about 95 % of the required energy to produce aluminum from bauxite. Another issue is the amount of solid waste produced when using primary aluminum. It is suggested that the solid waste generated per ton of secondary aluminum is 90 % lower than that of primary aluminum [7]. Moreover, it was estimated that one ton of recycled aluminum could save up 8 metric tons of bauxite, 6300 l of oil, and 7.6 m^3 of landfill [7]. In addition, the amount of greenhouse gas emissions is reduced by more than 95 % when recycling aluminum rather than extracting it from ore metal [8].

In this study, High Entropy Alloy (HEA) is used as the alloying element as there are some challenges associated with producing new HEA. High entropy alloy has multiple metallic materials combined together. It consists of four or more elements in a high or equal fraction [9]. There are 72 metallic elements that could be used to develop HEA, and identifying which elements to use and what concentration to use for each element is a challenge. It is a very complex optimization process, and many tests and experiments are required to find optimal HEA alloys with the required properties. In addition, melting is the primary method of mixing alloys, and melting different elements simultaneously to combine them is a challenge because they have different properties in terms of melting points, boiling points, densities, and volatility. Besides, the complexity of different elements with different properties leads to different solidification paths and phase transformation. Solidification pathways need to be carefully controlled to get a successful casting of HEA [10].

Aluminum cast alloys do not usually have the required properties that could be used for real applications. Therefore, the heat treatment process is performed to improve the properties of cast alloys, especially strength and ductility. One of the main heat treatment methods for aluminum and magnesium alloys is the T6 heat treatment which includes solution heat treatment and quenching in water followed by aging [11]. The solution and aging temperatures and time greatly influence the microstructure and properties of aluminum alloys. For example, the hardness of Al-Si-Cu alloy that was T6 heat-treated for 5 h had a hardness lower than that of the one heat-treated for 8 h [12]. Solution treatment aims to dissolve all of the alloying elements into the solution. The aging process aims to allow some alloying elements to start precipitating, which act as barriers for dislocation movement that results in the improvement of hardness strength [13].

The aluminum scrap and high entropy alloy were cast by the squeeze casting process. After the casting was completed, the mechanical properties and microstructure of the produced alloy were examined. Tensile, hardness, compression, and wear tests were conducted for the produced alloy. SEM was used to analyze the microstructure of the produced alloy, while XRD was used to analyze the elements and the phases present in the produced alloy. Moreover, T6 heat treatment was done for the produced alloy, including two main steps: solution treatment and aging. After that, the mechanical properties test and microstructure analysis were completed in order to compare the results before and after heat treatment.

2. Materials and methods

2.1. Sustainability

Sand casting, die gravity casting, and stir squeeze casting were compared to determine the most sustainable method in terms of eight parameters. These parameters are compressive strength, tensile strength, hardness, wear, porosity, health and safety, energy consumption, and lead time. The level of importance is not the same for all parameters, and to determine the level of importance of each parameter, the Analytical Hierarchy Method (AHP) was used. First, three experts were asked to complete a survey as in the 8 × 8 matrix (Eq.(1)):

$$Bl = \begin{pmatrix} P11l & P12l & ... & P1nl \\ P21l & P22l & ... & P2nl \\ ... & ... & ... & ... \\ Pn1l & Pn2l & ... & Pnnl \end{pmatrix}, \qquad (1)$$

Table 1. Importance scale of criteria for pairwise comparison

Value	Definition		
1	i and j are equally important		
3	i is slightly more important than j	1/3	i is slightly less important than j
5	i is more important than j	1/5	i is less important than j
7	i is much more important than j	1/7	i is much less important than j
9	i is absolutely more important than j	1/9	i is absolutely less important than j
2, 4, 6, 8	Intermediate values	1/2, 1/4, 1/6, 1/8	Intermediate values

where B is the matrix of the completed 8 × 8 matrix survey for each expert, and P is the comparison score given by the experts as described in Table 1. After that, the survey responses from the experts were unified into one matrix using the geometric mean technique as in Eq. (2); this step is done to convert the three matrices from the three experts into one general matrix:

$$X_{ij} = \sqrt[l]{\prod_{l=1}^{l} P_{ij} l}, \tag{2}$$

where X is the completed 8 × 8 matrix survey after all the three matrices were unified into one matrix.

The unified matrix then was normalized using Eq. (3):

$$y_{ij} = \frac{x_{ij}}{\sqrt{\left(\sum_{i=1}^{n} x_{ij}^2\right)}}, \tag{3}$$

where y is unified matrix after it was normalized. The normalization is important in order to change the different values for the different parameters to a standard scale because the parameters have different units.

After that, the weight percentages of these parameters were used to determine the most sustainable casting method. Scores were given for all eight parameters for the three casting methods. Based on a literature review, the scores were given within a range of 1–3. Mechanical properties such as tensile strength, wear, and hardness were found to be better for stir-squeeze casting. Therefore, they were given a higher score while porosity was higher for sand casting. Compressive strength scores were given based on porosity, where it was assumed that the lower the porosity, the higher the compressive strength. Energy consumption scores were given considering that stir-squeeze casting has three sources that consume energy. They are the melting furnace, stirrer motor, and hydraulic press. However, the only energy consumption source in gravity and sand casting is melting; therefore, they were given better scores than stir-squeeze casting. The health and safety parameter in stir-squeeze casting was given a higher score than the other two casting methods because the equipment used for this process has a runway that directly transfers the molten metal from the furnace to the die, while in sand and gravity casting, the molten metal is manually transferred to the die:

$$W_i = \frac{\sum_{i=1}^{n} y_{ij}}{\sum_{i=1}^{n}\sum_{j=1}^{n} y_{ij}}, \tag{4}$$

where W is the weight percentage for each of the 8 parameters, which determines the level of importance of each parameter when compared with the other parameters.

To confirm that the AHP method used is consistent, a consistency check was required for which Eq. (5) is used. CR needs to be less than 0.1 for the method to be consistent. The RI value is 1.41 because there are parameters [14]:

$$CR = \frac{CI}{RI}, \tag{5}$$

where CR is consistency ratio, CI is consistency index, and RI is the random consistency index. CI and $\lambda_{\max}$ are calculated using Eqs. (6) and (7):

$$CI = \frac{\lambda_{\max} - n}{n - 1}, \tag{6}$$

where $\lambda_{\max}$ is calculated using the following equation:

$$\lambda_{\max} = \frac{\sum_{j=1}^{n} X_{ij} W_j}{W_i}. \tag{7}$$

2.2. Alloy composition and material processing

The alloying material is a HEA produced through the powder metallurgy route. The composition of this alloy is $Al_{35}Li_{20}Mg_{15}Si_{10}Zn_{15}Ca_5$ 40 g (2.6 %). This HEA was converted into a powder using a ball mill. The primary material is LM25 (A356), comprising

Table 2. Elemental composition of LM25 + HEA alloy

	Al	Si	Fe	Cu	Mn	Mg	Ni	Pb	Zn	Ti	Li	Ca
wt (g)	1384.25	109	7.5	1.5	4.5	12	1.5	1.5	7.5	0.75	8	2
(wt.%)	89.88636	7.077922	0.487013	0.097403	0.292208	0.779221	0.097403	0.097403	0.487013	0.048701	0.519481	0.1287

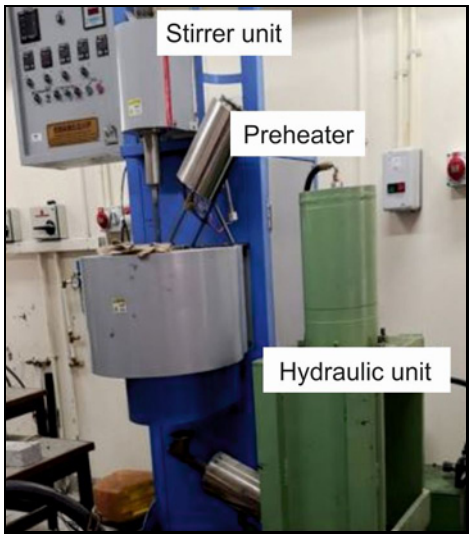

Fig. 1. Stir squeeze casting process used to produce the LM25 + HEA alloy.

1.5 kg of its weight. The composition of the produced alloy is shown in Table 2.

Stir squeeze casting equipment from SWAMEQUIP, as shown in Fig. 1, was employed to produce the aluminum alloy. The scrap aluminum was loaded into the crucible that was turned to 900 ℃. After that, the HEA was added to the molten metal by wrapping it in an aluminum foil and then inserted into the crucible. Then, the stirrer was started at a speed of 525 rpm for 5 minutes. Next, the molten metal was transferred to the die through a preheated runway to 750 ℃. After the molten metal filled the die, a pressure of 100 MPa was applied for 45 s.

2.3. Density and porosity calculations

To calculate the porosity using Eq. (8), experimental ($p_{\text{experimental}}$) and theoretical ($p_{\text{theoretical}}$) densities needed to be measured and calculated [15]:

$$\text{Porosity} = 1 - \left(\frac{p_{\text{experimental}}}{p_{\text{theoretical}}}\right) \times 100. \qquad (8)$$

Equation (9) was used to calculate the theoretical density of the developed alloy:

$$(\rho_{\text{LM2+HEA}})_{\text{theoretical}} = \\ = \text{VOL}_{\text{LM25}}\rho_{\text{LM25}} + \text{VOL}_{\text{HEA}}\rho_{\text{HEA}}, \qquad (9)$$

where VOL_{LM25} is the volume percentage of LM25, ρ_{LM25} is the density of LM25, VOL_{HEA} is the volume percentage of the HEA, and ρ_{HEA} is the density of the HEA.

Experimental density was determined by measuring the volume of the four cylinders that were cut from the produced alloy. The height and the diameter of each cylinder were measured using a digital Vernier caliper at four different positions. The average volume was then determined, after which the average experimental density was determined.

2.4. Characterization techniques

Cubes of 10 × 10 were cut for the optical microscope, and then an automated mounting press (SimpleMet1000, Buehler, USA) was used to create a circular mount for both samples. Before using the microscope, the samples needed to be ground, polished and etched. For grinding and polishing, an automated grinder-polisher was used (EcoMet 250 Pro, Buehler, USA). The samples were mechanically ground for 1.5 min using 400, 600, and 1200 grit abrasive paper. Then, polishing was completed in three stages using diamond suspension 9, 3, and 1 µm (Buehler, USA), with each stage lasting 5 min. After that, the specimens were placed in an optical microscope, and the focus was adjusted to get clear images. In addition, the microstructure and elemental analysis were studied using Field Emission Scanning Electron Microscope (FESEM) with an attached Energy Dispersive Spectroscopy (EDS) model JSM-7600F (JEOL, Japan). Moreover, X-ray diffraction analysis (XRD) was conducted Using X'pert PRO XRD (Malvern Panalytical Ltd, UK) with Cu Kα radiation ($\lambda = 1.5418$ Å). The specimen used for XRD is a circular disc with a diameter of 30 mm and a thickness of 3 mm.

After that, mechanical properties tests (hardness, tensile test, compression test, and wear test) were conducted. Rockwell hardness was measured using the indentation technique by a universal hardness tester UH250 (INDENTEC, USA). A force of 100 kgf was applied gradually to determine the Rockwell hardness number (HRB) using a 1/16" ball indenter with a dwell time of 15 s. The compression test was conducted using a 100 kN Universal testing machine (MTS 20/MH, France). Cylindrical samples were prepared to perform the test with a height of 25 mm and 13 mm diameter as per the ASTM E9. The compres-

sion load was applied gradually with a crosshead speed of 1 mm min^{-1} or 8.33 × 10^{-3} s^{-1} until the specimen was reduced to half of its original length or shears. The specimens were cut according to ASTM E8 standards for the tensile test. The sub-size specimen was used with the dimensions shown in Fig. 2. A 50 KN H50KT--0175 (Tinius Olsen, England) tensile testing machine was used for the tests. The specimen was gripped from the two ends, and the tensile load was applied gradually with a strain rate of 8.33 × 10^{-4} s^{-1}.

Besides, the wear test was conducted on a rotary tribometer pin on a disc wear testing machine (Ducom Instruments, India) as per the ASTM standard G99--17. The specimens were cut from the developed alloy using Wire EDM. The wear test specimen is a cylindrical pin with a diameter of 10 mm and 30 mm in height. The weight of the cylinder was measured before the test. The test specimen was inserted into the holding device perpendicular to the rotating steel disc with a 50 mm diameter. After that, a load of 10 N was applied to the holder, and then the rotation was started. The rotational speed was 382 RPM (2 m s^{-1}) for 1000 s. After that, the weight of the specimen was measured to detriment the weight loss.

T6 heat treatment was done for part of the produced casting. T6 heat treatment is usually used for aluminum to improve its mechanical properties [13]. An N7/H NABERTHERM heating furnace (Germany) was used to complete the T6 heat-treatment process. This process includes two main steps: solution treatment and aging. The metal was heated to 525 ℃ for 9 h and then directly quenched into the water during the first step. The alloy was heated to 175 ℃ for 6 h and cooled in the air in the second step.

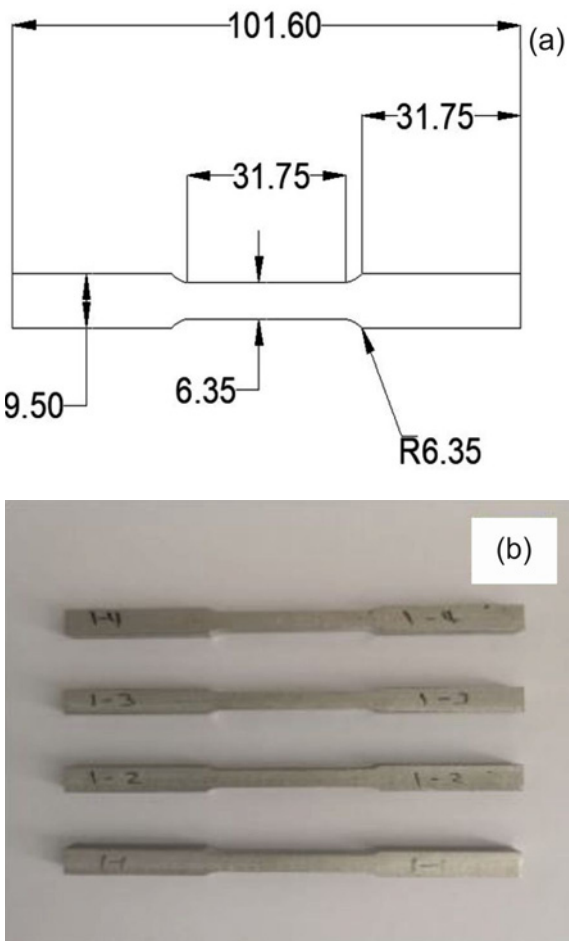

Fig. 2. (a) Tensile test specimen dimensions and (b) 4 tensile test specimens cut using wire EDM cutting machine.

3. Results and discussion

3.1. Sustainability

The AHP method was used to determine the level of importance of the selected eight parameters of suitability for the different casting methods. The AHP results showed that porosity (20.82 %) is the most important, followed by hardness (18.59 %) and wear (16.69 %). Table 3 shows the level of importance for all eight parameters. To check the consistency of the AHP method, the CR value was calculated. The CR value was determined to be 0.0457, which is lower than 0.1.

Table 3. Calculated weight percentage using the AHP method

Parameter	Weight percentage	Stir-squeeze casting	Gravity die casting	Sand casting
Porosity	20.82 %	1	3	3
Hardness	18.59 %	1	2	3
Wear	16.69 %	3	1	1
Compressive strength	15.30 %	3	2	1
Health and safety	12.44 %	3	2	1
Tensile strength	10.80 %	3	2	1
Energy consumption	2.91 %	1	2	3
Lead time	2.42 %	3	2	1
		2.587295666	1.90464218	1.412704334

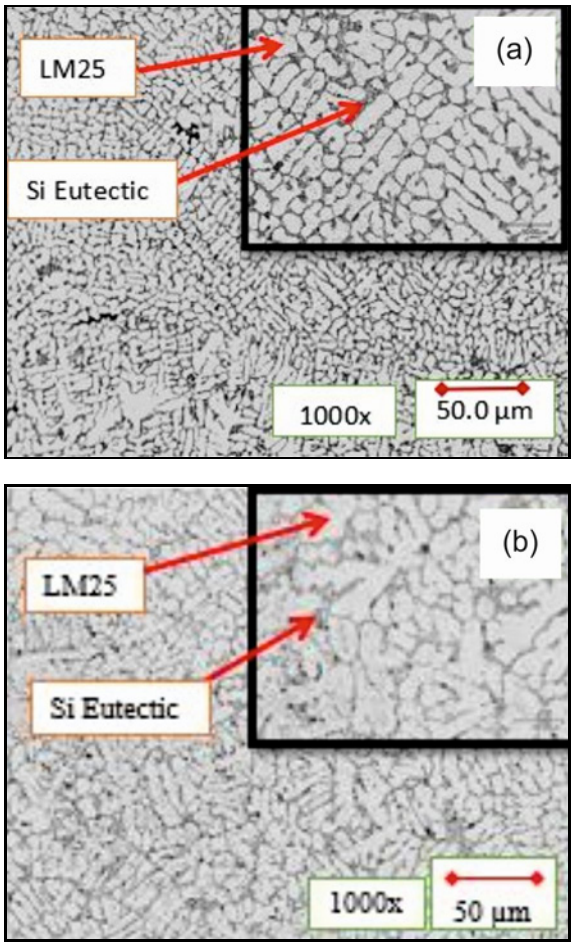

Fig. 3. Morphologies of the cast alloy scrap aluminum + HEA at 300× magnification: (a) before heat treatment and (b) after T6 heat treatment.

Therefore, the pairwise comparison matrix obtained from experts is consistent. The weight percentage was multiplied by the given scores for each casting method. After that, the final score for each casting method was calculated by adding all the rows together in each column, as shown in Table 3. The results showed that stir-squeeze casting has the highest score (2.58), followed by gravity casting (1.9) and then sand casting (1.4). Therefore, it was concluded that the stir squeeze casting method was the most sustainable among the three methods.

3.2. Microstructure and elemental analysis

The microscopic morphologies for the produced alloy are demonstrated in Fig. 3 at 300× magnification. Figure 3a shows the optical microscopic morphology for the cast alloy before heat treatment, while Fig. 3b shows the microscopic morphology for the produced alloy after T6 heat treatment. The white regions between grain boundaries are the scrap aluminum phase (LM25), and the eutectic phase of silicon appears on

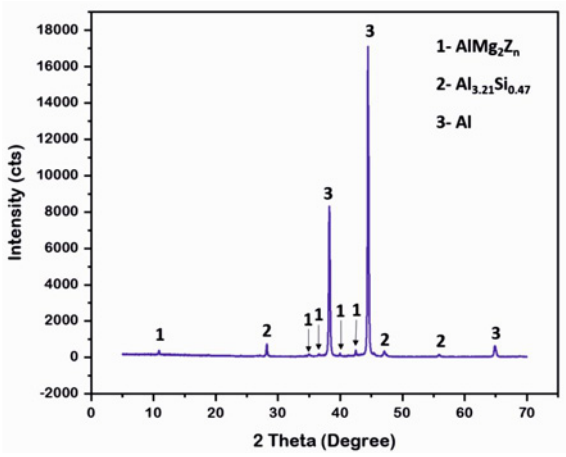

Fig. 4. XRD results for the LM25+ HEA show the presence of phases in the alloy.

the grain boundaries [16]. From the morphologies of the alloy, it seems that the alloy has low porosity (dark regions). Moreover, the aging process allowed fine Si particles to reappear in the aluminum matrix, which is also confirmed by the SEM elemental mapping [17].

Besides, the grain size decreased after heat treatment; the average grain size was 40.3 µm before heat treatment and 27.765 µm after the process. The grain size reduction can be attributed to the quenching process during solution treatment. The alloy was rapidly cooled during quenching, which did not give enough time for the grains or crystals to grow. In addition, a slight increase in porosity was reported after heat treatment. The porosity before heat treatment was found to be 1.064 %, and this is relatively small if compared to the original LM25 alloy. The porosity of A356 (LM25) varies between 0.5 and 1.5 %, depending on the location from the free end of the casting [18]. After heat treatment, the porosity was calculated to be 2.0466 %. One study compared the porosity of a die-cast aluminum alloy before and after heat treatment and reported that porosity increased after T6 heat treatment, affecting other mechanical properties [11]. There are entrapped gasses inside the alloy with high pressure that form the porosities, and they regrow when exposed to high temperatures [19].

The presence of the Si eutectic phase is also shown in the elemental mapping. The Si particles were all accumulated in the grain boundaries. Al and Si are the most common elements, both before and after heat treatment, but other elements, such as O and Zn, were also present in smaller percentages, and they were uniformly distributed in the mixture. Before heat treatment, the Si eutectic phase is accumulated in the grain boundaries, but after heat treatment, the Si eutectic phase appears to be redistributed and more uniform where it can be seen mixed with the aluminum matrix. Besides, the XRD (see Fig. 4) results showed alu-

minum has the highest peaks since it is the primary material. However, other elements such as O, Zn, and Si are also present. Along with these elements, peaks of intermetallic phases of $Al_{3.21}Si_{0.47}$ and $AlMg_2Zn$ were also present. The appearance of such phases in the grain boundaries of the alloy affects the fracture type and properties of the alloy.

The SEM morphology image in Fig. 5 demonstrates the appearance of the Si eutectic phase more clearly in the grain boundaries. Pores are rarely found from the SEM morphology, which indicates low porosity existence, confirmed by the porosity calculations. After heat treatment, the Si eutectic phase accumulated along the grain boundaries, but the distribution appeared to be more uniform than before heat treatment. As shown in Fig. 5b, the Si eutectic phase after T6 was transferred to a polyhedral form that appears to be discontinuous [20].

3.3. Mechanical properties

3.3.1. Tensile test

The average tensile strength was 159.9 MPa. This is relatively sufficient compared to precipitation-treated LM25 with a tensile strength of 160–200 MPa produced by gravity casting [21]. However, this is heat-treated, and the tensile strength of the cast alloy would be lower. A composite of LM25 + Al_2O_3 tensile strength was found to be 125 MPa, which is relatively lower than the tensile strength of the produced alloy. The alloy appears to be brittle, where little ductility was observed in the stress vs. strain curve as in Fig. 6, as the average elongation was only 0.426 %. One specimen was tested after T6 heat treatment, as shown in the black curve in Fig. 6. It is important to notice the tensile equipment did not start the stresses from zero because of pre-tension, but the tensile behavior of the alloy is not affected by this issue. The tensile strength was obtained to be 159.2 MPa, which is almost the same as the average obtained before heat treatment. Testing more samples might give a clearer picture of the tensile strength. The alloy still behaved as a brittle material after the T6 heat treatment and even had lower elongation than the average obtained before the heat treatment process.

3.3.2. Compression test

The average compressive strength was reported to be 383.87 MPa at a force of 51 kN. LM25 + Al_2O_3 ultimate compression strength was found to be 312 MPa in one study, indicating that the produced alloy has higher compressive strength than this aluminum composite [16]. The average deflection was calculated to be 7.1 mm before fracture. The relatively good compressive strength is attributed to the small grain size

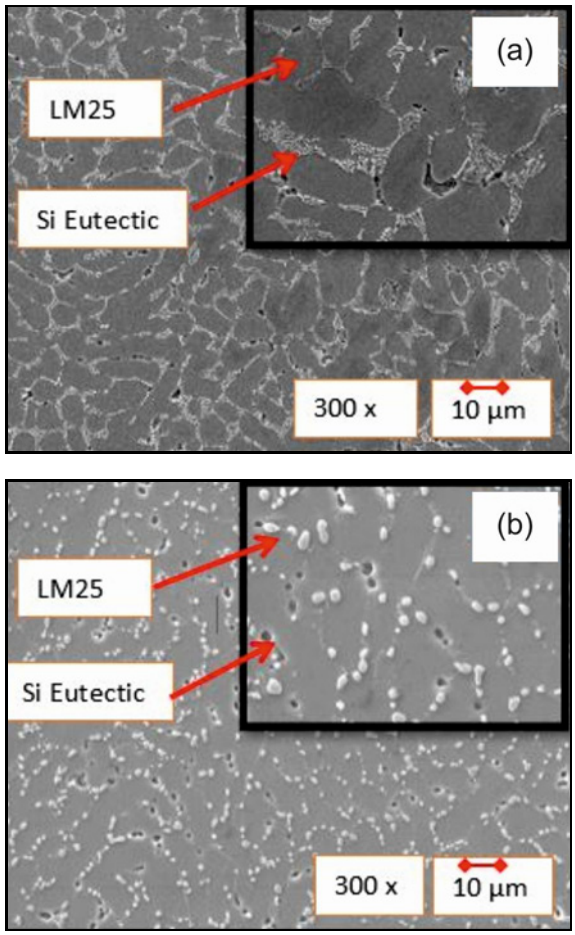

Fig. 5. SEM image of the cast alloy scarp aluminum + HEA at 300× magnification and 1000× magnification, (a) before heat treatment and (b) after heat treatment.

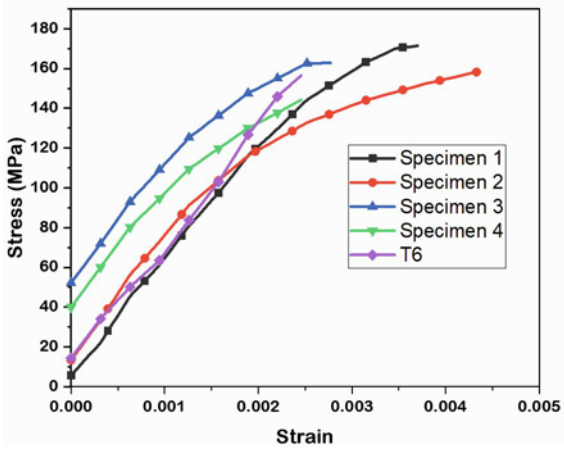

Fig. 6. Stress-strain graph for the tensile test for the LM25 + HEA for all specimens before teat treatment and after heat treatment.

and appearance of the second phases, especially in the grain boundaries. Moreover, it is noticeable that

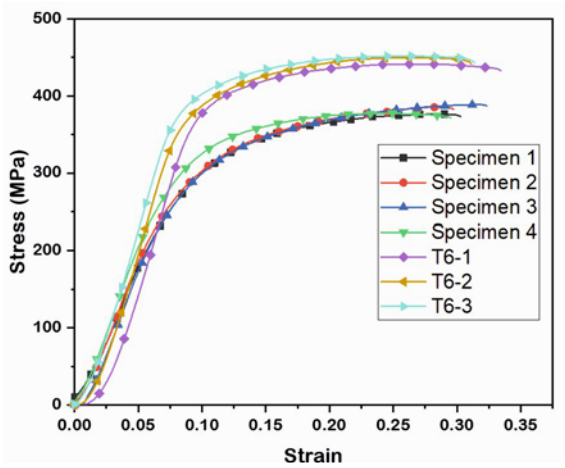

Fig. 7. Stress-strain graph for compression test for the LM25+HEA alloy before and after T6 heat treatment.

compressive strength is significantly higher than the tensile strength, making this alloy more suitable for applications that require better compressive strength, such as car wheels. LM25 usually has good compressive strength because it is much higher than its tensile strength [22]. The compression test was also done for the alloy after heat treatment. There was a significant improvement in the compressive strength, averaging 447.79 MPa, which is significantly higher than before heat treatment. This significant improvement results from the redistribution of the Si eutectic phase along with the precipitation of Si particles in the aluminum matrix after the aging process. The average deflection was 6.51 mm, which is slightly lower than before heat treatment, and that might be attributed to the reduction in grain size. Figure 7 shows the stress vs. strain graph for the compression test for all 4 specimens before heat treatment and 3 specimens after T6 heat treatment, where it clearly shows the improvement in yield and compressive stress after T6.

3.3.3. Hardness

Rockwell hardness test was conducted for the same sample of the optical microscope. The average value obtained was 55.8 HRB. This value is consistent with the Rockwell hardness of LM25, which ranges between 30–80 HRB [21]. If compared with aluminum composites, the obtained hardness values are lower. For instance, a composite of A365(LM25) + Al_2O_3 has a hardness value of 70 HRB [23]. The low porosity of the produced alloy was significant in increasing the hardness value [16]. The Rockwell hardness was also tested after the T6 heat treatment, and the average Rockwell hardness was obtained to be 75.75 HRB. The hardness of the alloy increased significantly after heat treatment. The perception of Si particles after the aging process played a significant role in increasing the hardness value.

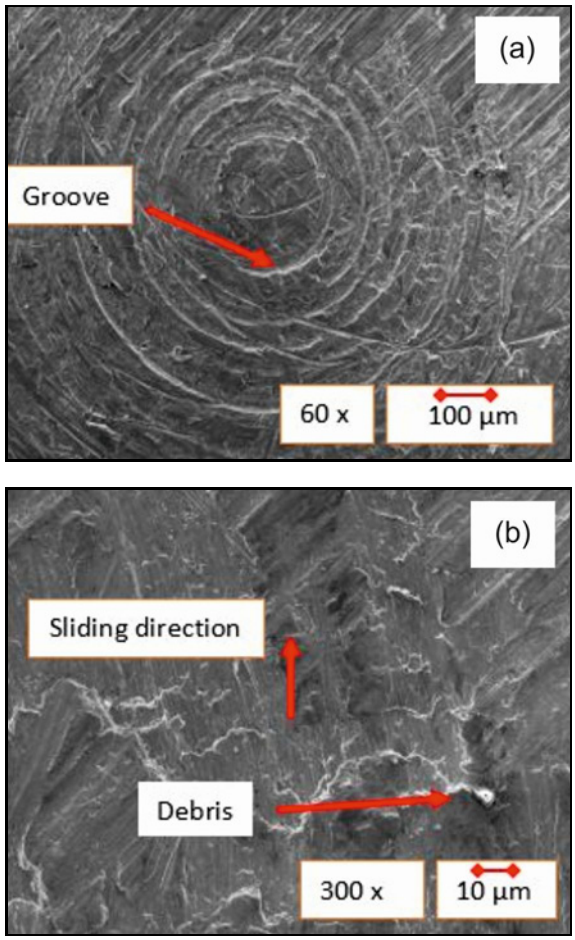

Fig. 8. SEM morphologies of the worn-out surface: (a) × 60 and (b) × 300.

3.3.4. Abrasion wear

The average weight loss was found to be 0.003395 g. In the same testing conditions, wear loss for pure LM25 alloy was reported to be 0.016 g. Similarly, with the same testing conditions for an LM25 + B4C composite, wear loss was slightly lower than that of pure LM25 [24]. Figure 8 shows the SEM morphologies of the worn surface. The appearance of grooves demonstrates material loss. In addition, there appears to be some debris where fragments of materials such as iron were also confirmed by the EDS analysis. Table 4 shows a summary of the EDS in three different areas. It is clear that carbon is present in all spectra. Iron can be seen more clearly in spectrum 3, which is 2.6 % of the total elements. The appearance of iron in some areas in the wear track is attributed to the mechanical mixing during the contact between the pin and the steel disc [25]. The presence of carbon in high percent-

Table 4. Summary of EDS element analysis at 3 different spectra

	Al	O	C	Si	Fe	Mg	Zn
Spectrum 1	69.8 %	6.4 %	16.3%	4.4 %	0.6 %	1.4 %	1.0 %
Spectrum 2	75.2 %	3.8 %	13 %	5.1 %	0.6 %	1.3 %	1.0 %
Spectrum 3	49.8 %	28.9 %	14 %	3.1 %	2.6 %	1.1 %	0.6 %

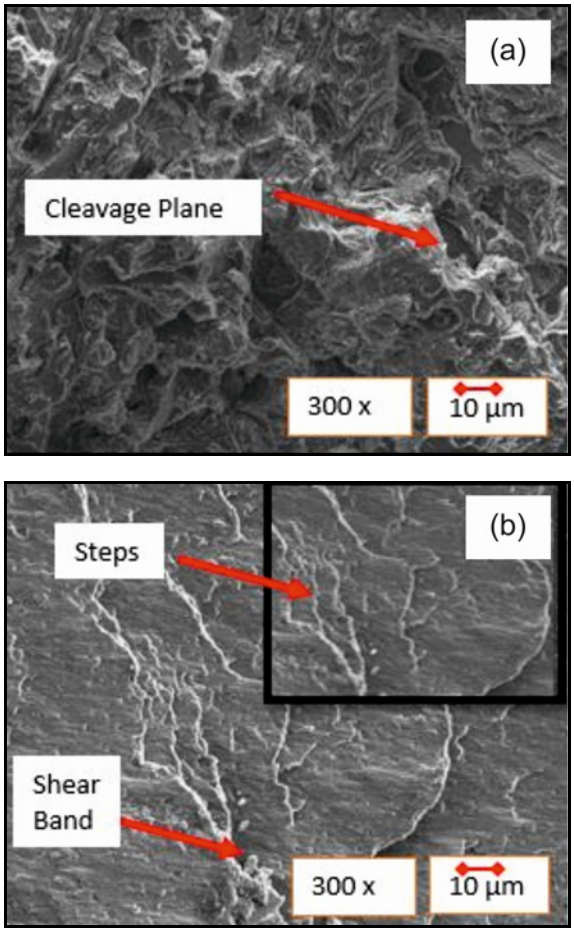

Fig. 9. SEM morphologies for tensile (a) and compression (b) fractures.

ages is because of forming a carbonaceous layer on the worn surface [25].

3.3.5. Fractured surface analysis

The failure appears to be brittle from the SEM morphologies for both tensile and compression fractures and starts at the grain boundaries. Decohesion of the dendrites caused the failure of the material during the compression and tensile tests. The arrows in Fig. 9a show the grain boundaries where the cleavage fracture is estimated to start. The reason that the fracture accrued at the grain boundaries is the presence of second phases such as $Al_{3.21}Si_{0.47}$ and $AlMg_2Zn$. Such phases have weak bonding with the matrix, which causes the decohesion in the grain boundaries [26]. The fracture surface of the sheared specimen after compression is shown in Fig. 9b, where the arrow indicates the shear band. The shear cracking region appears to be composed of different cracking facets with different layers, which form steps that are the translamellar shear cracking facets [27].

4. Conclusions

– Applying the AHP method revealed that porosity, hardness, and wear resistance were the most important parameters when comparing sand casting, gravity, and stir-squeeze casting.

– Applying the concept scoring method indicated that the stir-squeeze casting is the best method among the three methods.

– The SEM and optical microscope showed the appearance of the Si eutectic phase in the grain boundaries both before and after heat treatment, which was also confirmed by the elemental mapping.

– The Si eutectic phase after heat treatment was more uniformly distributed where the Si particle appeared inside the grains with the aluminum matrix.

– From XRD results, the secondary phases such as $Al_{3.21}Si_{0.47}$ appeared, confirming the existence of the Si eutectic phase in the grain boundaries.

– The average tensile strength was reported to be 159.9 MPa before heat treatment, and there was no noticeable change after the heat treatment.

– The hardness increased significantly after T6 heat treatment, where it was 55.8 HRB before heat treatment and 75.75 HRB after heat treatment.

– There was a significant increment in compressive strength where the average was 383.87 MPa before heat treatment and 447.49 MPa after heat treatment.

– The significant improvement in hardness and compressive strength is attributed mainly to the precipitation hardening where Si particles formed in the aluminum matrix after the aging process and the reduction in grain size.

– The alloy was found to be brittle before and after heat treatment, which was noticed by the SEM images of the fractured surface where cleavage fracture was noticed.

– The main reason for the brittle fracture is the

appearance of secondary phases in the grain boundaries.

– It is recommended to implement a process that will improve the ductility, such as hot rolling.

The wear test results showed that the average wear loss is 0.003395 g, which is relatively better when compared to LM25.

– After the appropriate heat treatment process, it can be recommended that the produced alloy can be used to manufacture car wheels.

Acknowledgement

We would like to acknowledge the contribution of the late Dr. Ramanathan Arunachalam.

References

[1] S. N. A. Safri, M. T. H. Sultan, M. Jawaid, K. Jayakrishna, Impact behaviour of hybrid composites for structural applications: A review, Compos. Part B Eng. 133 (2018) 112–121. https://doi.org/10.1016/j.compositesb.2017.09.008

[2] K. L. Fan, G. Q. He, X. S. Liu, B. Liu, M. She, Y. L. Yuan, Y. Yang, Q. Lu, Tensile and fatigue properties of gravity casting aluminum alloys for engine cylinder heads, Mater. Sci. Eng. A 586 (2013) 78–85. https://doi.org/10.1016/j.msea.2013.08.016

[3] M. V. Santosh, K. R. Suresh, S. Kiran Aithal, Mechanical characterization and microstructure analysis of Al C355.0 by sand casting, die casting and centrifugal casting techniques, Mater. Today Proc. 4 (2017) 10987–10993. https://doi.org/10.1016/j.matpr.2017.08.056

[4] M. O. Adeoti, M. S. Abolarin, K. A. Olaiya, B. Bongfa, Comparison of the mechanical properties of sand and gravity die cast aluminium scraps, Int. J. Engg. Res. & Sci. & Tech. 4 (2015) 37–43.

[5] C. K. Zheng, W. W. Zhang, D. T. Zhang, Y. Y. Li, Low cycle fatigue behavior of T4-treated Al-Zn-Mg-Cu alloys prepared by squeeze casting and gravity die casting, Trans. Nonferrous Met. Soc. China 25 (2015) 3505–3514. https://doi.org/10.1016/S1003-6326(15)63992-9

[6] Y.-H. Seo, C.-G. Kang, The effect of applied pressure on particle-dispersion characteristics and mechanical properties in melt-stirring squeeze-cast SiC$_p$/Al composites, J. Mater. Process. Technol. 55 (1995) 370–379. https://doi.org/10.1016/0924-0136(95)02033-0

[7] S. Capuzzi, G. Timelli, Preparation and melting of scrap in aluminum: A review, Metals 8 (2018) 249. https://doi.org/10.3390/met8040249

[8] J. Cui, H. J. Roven, Recycling of automotive aluminum, Trans. Nonferrous Met. Soc. China 20 (2010) 2057–2063. https://doi.org/10.1016/S1003-6326(09)60417-9

[9] Z. Li, A. Ludwig, A. Savan, H. Springer, D. Raabe, Combinatorial metallurgical synthesis and processing of high-entropy alloys, 33 (2018) 3156–3169. https://doi.org/10.1557/jmr.2018.214

[10] J. Bishop-Moser, D. Miracle, Manufacturing High Entropy Alloys: Pathway to Industrial Competitiveness, Technical Report, Foresight: Alliance for Manufacturing Foresight, 2018. https://hdl.handle.net/2027.42/146747

[11] A. Niklas, S. Orden, A. Bakedano, M. Silva, E. Nogués, A. I. Fernández-Calvo, Effect of solution heat treatment on gas porosity and mechanical properties in a die cast step test part manufactured with a new AlSi10MnMg(Fe) secondary alloy, Mater. Sci. Eng. A 667 (2016) 376–382. https://doi.org/10.1016/j.msea.2016.05.024

[12] X. Li, H. Yan, Z. Wang, N. Li, J. Liu, Q. Nie, Effect of heat treatment on the microstructure and mechanical properties of a composite made of Al-Si-Cu-Mg aluminum alloy reinforced with SiC particles, Metals 9 (2019) 1205. https://doi.org/10.3390/met9111205

[13] D. Pye, The heat treatment of aluminum alloys, (2018). https://themonty.com/the-heat-treatment-of-aluminum-alloys, (accessed January 13, 2020).

[14] M. Piantanakulchai, N. Saengkhao, Evaluation of alternatives in transportation planning using multi-stakeholders multi-objectives AHP modeling, Proc. East. Asia Soc. Transp. Stud. 13 (2003) 1613–1628.

[15] S. P. Dwivedi, S. Sharma, R. K. Mishra, Microstructure and mechanical behavior of A356/SiC/Fly-ash hybrid composites produced by electromagnetic stir casting, J. Brazilian Soc. Mech. Sci. Eng. 37 (2014) 57–67. https://doi.org/10.1007/s40430-014-0138-y

[16] P. K. Krishnan, J. V. Christy, R. Arunachalam, A. H. I. Mourad, R. Muraliraja, M. Al-Maharbi, V. Murali, M. M. Chandra, Production of aluminum alloy-based metal matrix composites using scrap aluminum alloy and waste materials: Influence on microstructure and mechanical properties, J. Alloys Compd. 784 (2019) 1047–1061. https://doi.org/10.1016/j.jallcom.2019.01.115

[17] A. Fabrizi, S. Capuzzi, A. De Mori, G. Timelli, Effect of T6 heat treatment on the microstructure and hardness of secondary AlSi9Cu3(Fe) alloys produced by semi-solid SEED process, Metals 3 (2018) 750. https://doi.org/10.3390/met8100750

[18] K. D. Li, E. Chang, A mechanism of porosity distribution in A356 aluminum alloy castings, Mater. Trans. 43 (2002) 1711–1715. https://doi.org/10.2320/matertrans.43.1711

[19] S. Tammas-Williams, P. J. Withers, I. Todd, P. B. Prangnell, Porosity regrowth during heat treatment of hot isostatically pressed additively manufactured titanium components, Scripta Materialia 122 (2016) 72–76. https://doi.org/10.1016/j.scriptamat.2016.05.002

[20] R. Gecu, S. Acar, A. Kisasoz, K. Altugguler, A. Karaaslan, Influence of T6 heat treatment on A356 and A380 aluminium alloys manufactured by thixoforging combined with low superheat casting, Trans. Nonferrous Met. Soc. China 28 (2018) 385–392. https://doi.org/10.1016/S1003-6326(18)64672-2

[21] Hall and Botterill Cast Aluminum Products, LM25 ALUMINIUM CASTING ALLOY, (2018). https://www.gutter.co.uk/wp-content/uploads/2018/05/LM25-ALUMINIUM-CASTING-ALLOY1.pdf

[22] N. S. Devoor, D. Ramesh, S. Awarasang, Study of the tensile and compression behaviour of LM 25 alu-

minium alloy reinforced with steel wire, Int. J. Innov. Res. Dev. (2016) 65–69.
[23] R. Arunachalam, P. Kumar, R. Muraliraja, A review on the production of metal matrix composites through stir casting – Furnace design, properties, challenges, and research opportunities, Journal of Manufacturing Processes 42 (2019) 213–245. https://doi.org/10.1016/j.jmapro.2019.04.017
[24] V. Suresh, P. Vikram, R. Palanivel, R. F. Laubscher, Mechanical and wear behavior of LM25 aluminium matrix hybrid composite reinforced with boron carbide, graphite and iron oxide, Mater. Today Proc. 5 (2018) 27852–27860. https://doi.org/10.1016/j.matpr.2018.10.023
[25] H. Singh, H. Bhowmick, Lubrication characteristics and wear mechanism mapping for hybrid aluminium metal matrix composite sliding under surfactant functionalized MWCNT-oil, Tribol. Int. 145 (2020) 106152. https://doi.org/10.1016/j.triboint.2019.106152
[26] M. Lalpoor, D. G. Eskin, G. ten Brink, L. Katgerman, Microstructural features of intergranular brittle fracture and cold cracking in high strength aluminum alloys, Mater. Sci. Eng. A 527 (2010) 1828–1834. https://doi.org/10.1016/j.msea.2009.11.003
[27] R. Cao, L. Li, J. H. Chen, J. Zhang, Study on compression deformation, damage and fracture behavior of TiAl alloys: Part II. Fracture behavior, Mater. Sci. Eng. A 527 (2010) 2468–2477. https://doi.org/10.1016/j.msea.2008.12.012